Ceramics International xxx (xxxx) xxx–xxx

Contents lists available at ScienceDirect

Ceramics International

journal homepage: www.elsevier.com/locate/ceramint

Low-temperature exfoliated graphene oxide incorporated with different types of natural rubber latex: Electrical and morphological properties and its capacitance performance

M.D. Nurhafizah[a,*], A.A. Aziz[a], A.B. Suriani[c,d], A. Mohamed[c,e], T. Soga[f]

[a] Nano-Optoelectronics Research and Technology Laboratory, School of Physics, Universiti Sains Malaysia, 11800, Minden Penang, Malaysia
[c] Nanotechnology Research Centre, Faculty of Science and Mathematics, Universiti Pendidikan Sultan Idris, 35900, Tanjung Malim, Perak, Malaysia
[d] Department of Physics, Faculty of Science and Mathematics, Universiti Pendidikan Sultan Idris, 35900, Tanjung Malim, Perak, Malaysia
[e] Department of Chemistry, Faculty of Science and Mathematics, Universiti Pendidikan Sultan Idris, 35900, Tanjung Malim, Perak, Malaysia
[f] Department of Frontier Materials, Nagoya Institute of Technology, Gokiso-cho, Showa-ku, Nagoya, 466-8555, Japan

ARTICLE INFO

Keywords:
B. Nanocomposites
C. Electrical conductivity
E. Electrodes

ABSTRACT

A simple with cost-effective method in the production and fabrication of graphene-based rubber nanocomposites as electrode materials is still remain a global challenge. In this work, we proposed one- and two-step approaches to fabricate an exfoliated graphene oxide (GO) as nanofiller in three different types of rubber latex polymer, namely, low ammonia natural rubber latex (NRL), radiation vulcanized NRL (RVNRL), and epoxy NRL 25 (ENRL 25). The electrical conductivity and capacitive behavior of nanocomposite samples were investigated under a four-point probe and cyclic voltammetry measurements, respectively. Meanwhile, the morphological properties were observed using field emission scanning electron microscopy, energy dispersive X-ray, optical polarization microscope, high-resolution transmission electron microscopy, Fourier-transform infrared spectroscopy, micro-Raman spectroscopy, and X-ray diffraction. The thermal stabilities of the nanocomposites were also investigated by thermogravimetric analysis. Among all, the GO/RVNRL polymer nanocomposite samples performed a better homogeneity with an improved electrical conductivity ($\sim 8.6 \times 10^{-4}$ Scm^{-1}) as compared with the GO/ENRL 25 ($\sim 3.1 \times 10^{-4}$ Scm^{-1}) and GO/NRL ($\sim 2.6 \times 10^{-4}$ Scm^{-1}) polymer nanocomposite samples. In addition, the GO/RVNRL polymer nanocomposite electrodes showed acceptable specific capacitance (5 Fg^{-1}). The successfully fabricated conductive GO-based rubber nanocomposites are suitable for new supercapacitor electrodes.

1. Introduction

The 1960s was the decade when the rising growth of the rubber-based industry [1,2]. Rubber-based products were a hot topic, especially in mechanical technology, due to their excellent elastic properties and mechanical strength [3]. Therefore, new revolutions in many fields, such as vehicle engineering, electronics, biomedicine, and aerospace industries, have attracted numerous researchers [4–6]. Milk liquid latex is originally harvested from the bark of the natural rubber tree or known as *Hevea brasiliensis* [7]. The isoprene monomer consisted in the latex polymer, which is good for its elasticity features and the double bonds in the backbone chain, has opened a window for the functionalization process. However, several imbalanced properties, especially in the dynamic mechanical and thermal properties, make the NRL polymer unpractical for other industry uses unless reinforced with nanofillers. Nanofillers with versatile surface characteristics, such as having an exceptional high mechanical strength, large surface area with high aspect ratio, and water-based, are highly needed [8,9].

Thus far, graphene (GE) is known to be a good nanofiller due to its electrical, mechanical, and optical properties [10,11]. Various methods have been used to synthesize GE [10–12]. Among a variety of methods, the production of GE via a wet chemical exfoliation route has gained numerous interests because it is readily-available in dispersions, easy for fabrication with other polymers, and susceptible for functionalization stages. However, GE suspensions in an aqueous solution contain a tremendous amount of oxygen functional groups, and it is called as graphene oxide (GO). To the best of our knowledge, instead of exploiting GO, the reduction of GO to rGO is more likely valuable in terms of electronic conjugation improvement. However, the low concentration and weak stability of rGO suspensions make GO the most preferable candidate as a nanofiller in electrode applications. In addition, GO is considered an ideal reinforcing and functional nanofiller due to its

* Corresponding author. Nano-Optoelectronics Research and Technology Centre, Universiti Sains Malaysia, 11800, Minden Penang, Malaysia.
E-mail address: mdnurhafizah@usm.my (M.D. Nurhafizah).

https://doi.org/10.1016/j.ceramint.2019.11.005
Received 11 September 2019; Received in revised form 28 October 2019; Accepted 1 November 2019

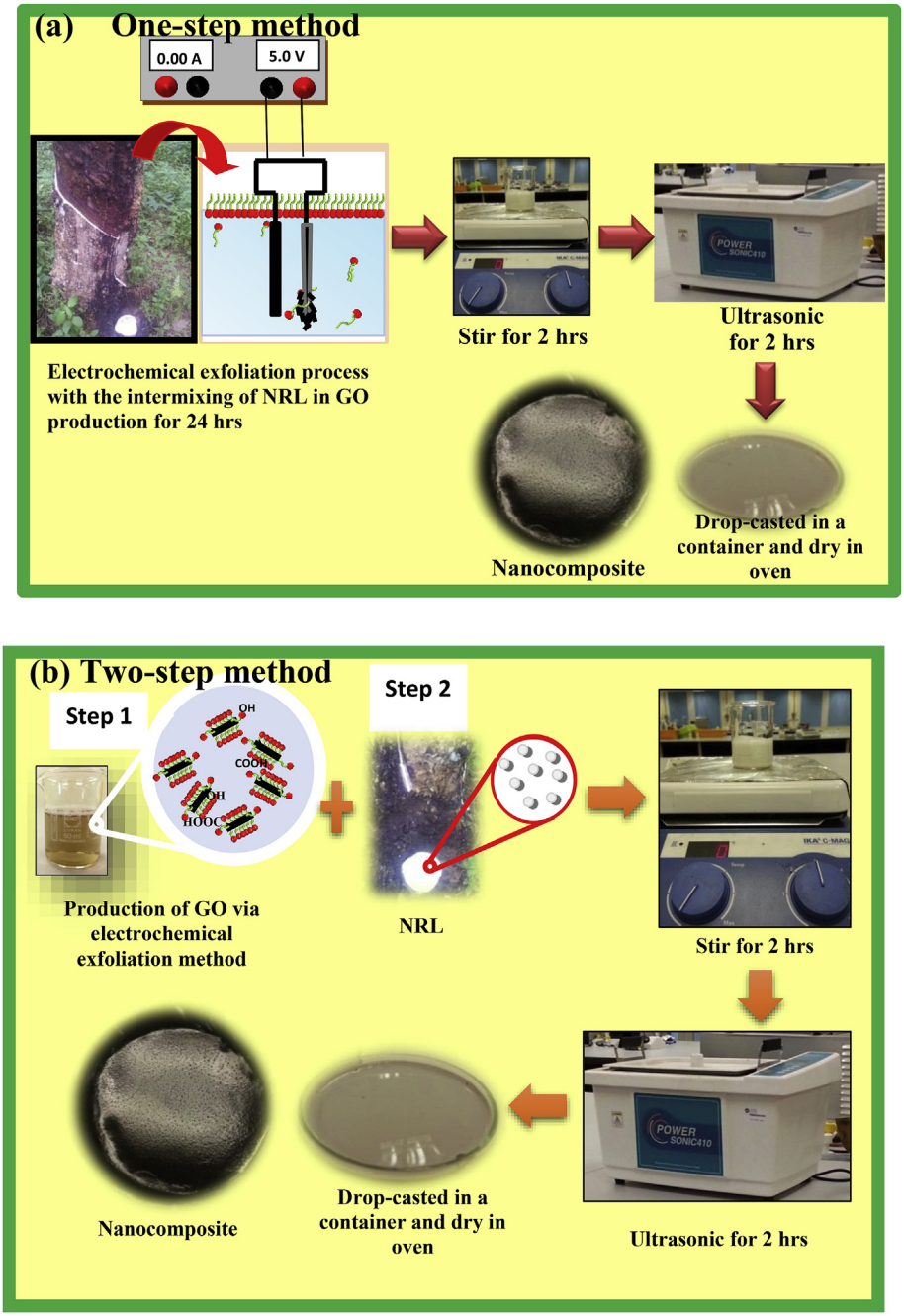

Fig. 1. The synthesis method of the GO/NRL polymer nanocomposites produced via (a) one-and (b) two-step methods, respectively.

chemical structures, and considerable research has been actively carried out since a decade ago [12]. Taking the advantages of GO, the use of GO in NRL may alter insulating polymers to conductive rubber nanocomposites.

Many commercial exploitations of GO-based/NRL composites have been widely practiced, including latex technology [13], melt compounding [14], solution mixing [15], and in situ polymerization [16]. However, these methods have several drawbacks, such as time consuming, difficult to control, tedious preparation procedure, and complex technology needed. Many review articles on GO-based rubber for nanocomposites covering various aspects, such as morphological properties, mechanical properties, and fracture behavior, have been published [17–19]. Earlier, we carried out a systematic investigation on GO/NRL and rGO/RVNRL nanocomposites as new electrodes for supercapacitors [20,21]. However, no report has been published with respect to the preparation of various types of NRL polymers, such as polar and non-polar rubbers. Interestingly, synthetic or polar NRL polymers also exhibit advantages, such as high mechanical strength due to a crosslinking agent.

Therefore, in this work, a comparison study was made for three different types of GO/NRL in terms of electrical conductivity and its effect to the capacitive behavior. Conductive GO/NRL, GO/RVNRL, and GO/ENRL25 polymer nanocomposites were prepared by incorporating GO suspensions with NRL via an electrochemical exfoliation and simple solution mixing approach for one- and two-step methods, respectively. However, the use of GO without a stabilization treatment can greatly reduce the dispersion level of the nanosize-scale materials in nanocomposites. Therefore, in this work, we still maintained the use of hyperbranched triple-tail surfactant, known as sodium 1,4-bis(neopentyloxy)- 3-(neopentyloxycarbonyl)-1,4-dioxobutane-2-sulphonate (TC14),

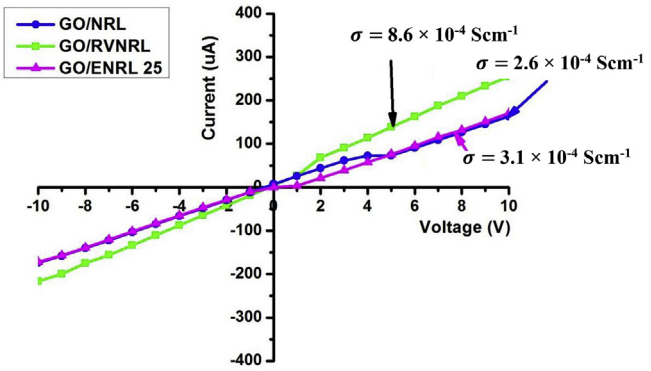

Fig. 2. *I–V* properties of the GO/NRL, GO/RVNRL, and GO/ENRL 25 polymer nanocomposites.

as previously reported [21]. The use of a TC14 surfactant is highly beneficial for the exfoliated, intercalated, and stabilized process of GO sheets in an aqueous solution via an electrochemical exfoliation method. The effects of the TC14-stabilized GO/NRL nanocomposites on the composites' morphological and electrical properties are investigated. This research greatly took advantage on the fabrication of new conductive supercapacitor electrodes from different types of NRL polymers.

2. Materials and methods

Two high-purity graphite rods (99.99%, Goodfellow Company, Germany) with a length and diameter of approximately 15.0 and 1.0 cm, respectively, were used. The polymers were collected from the Malaysian Institute of Nuclear Technology Research, Bangi, Malaysia. The RVNRL polymers were irradiated at RAYMINTEX Plant, with doses up to 12 kGy using γ-rays from a ^{60}Co gamma ray source at a constant dose rate (2 kGy/hour) for 6 h of radiation time. Meanwhile, the determination values for total solid content (TSC) and dry rubber content (DRC) of low-ammonia NRL were determined as per ISO 124: 1997 (E) and ISO 126: 1995 (E), respectively. The TSC and DRC values obtained were 33.87 ± 0.01% and 32.51 ± 0.08%, respectively. Meanwhile, 25 mol% of epoxidation was performed to the ENRL 25 polymer. The TSC of the ENRL 25 polymer was 47.28 ± 0.01%. The three NRL polymers were used without any purification.

2.1. Preparation of nanocomposites via one-and two-step methods

This study adopted one- and two-step methods for the fabrication of GO/NRL nanocomposites as reported in previous works [20,21]. Basically, the GO/NRL and GO/RVNRL nanocomposites implemented the one-step method via an electrochemical exfoliation approach. A 1:1 vol ratio between TC14-GO and NRL was used with an applied voltage of 7 V for a 24 h synthesis. The dispersion was then stirred (3000 rpm) and sonicated for 2 h before overnight cast drying. Meanwhile, the GO/ENRL 25 polymer nanocomposite was produced via a two-step method due to the inhomogeneous admixture observed at the initial preparation by the one-step method of electrochemical exfoliation technique (Supplementary). The resulting two phases of the GO/ENRL 25 admixture during the one-step method might be due to the additional epoxy group in the NRL structure, which brought an incompatible mixture to the home-made surfactant TC14. Similar procedures for the mechanical stirring and bath sonication of the GO/NRL polymer nanocomposite were carried out during the fabrication of the GO/ENRL 25 polymer nanocomposite. The overall procedures of the one- and two-step methods are shown in Fig. 1.

2.2. Characterizations

The initial analysis was performed by measuring the electrical properties of GO-filled NRL nanocomposites, followed by capacitance and morphological properties. Through this study, a standard four-point probe measurement (Keithley 2636A) was used for electrical testing. Meanwhile, the capacitance performance was measured using Gamry Potentiostat Series G750, USA). The nanocomposite samples were then analyzed using field emission scanning electron microscopy (FESEM) equipped with energy-dispersive X-ray (EDX) spectroscopy (Hitachi SU8020) with an operating voltage of 2–5 V, a standard optical polarizing microscopy (OPM) at Universiti Pendidikan Sultan Idris, and high-resolution transmission electron microscopy (HRTEM) (JEOL JEM-2100) with an accelerating voltage of 160 kV for surface observations. The investigations of the chemical properties of the nanocomposites were performed using Fourier-transform infrared spectroscopy (FTIR) (Nicolet Macna-IR760 spectrometer) within the region of 500–4000 cm^{-1}. For crystallinity measurements, micro-Raman spectroscopy (Renishaw inVia confocal Raman microscope) using an excitation of Ar^+ ion laser at 514 nm and X-ray powder (XRD) (PANalytical X'pert PRO XRD instrument) were employed. In addition, the effect of nanocomposites on the thermal stability was studied using thermogravimetric analysis (TGA)/SDTA 851 (Mettler-Toledo) under a nitrogen gas flow at 10 °C min^{-1} of heating rate.

3. Results and discussion

3.1. Electrical conductivity testing

Prior to the supercapacitor measurement, the electrical testing was performed to all prepared nanocomposite samples for electrical conductivity measurement. Fig. 2 shows the *I–V* curves for the samples. Surprisingly, among all nanocomposite samples, the *I–V* characteristic of GO/RVNRL showed the highest electrical conductivity (~8.6×10^{-4} Scm^{-1}), followed by GO/ENRL 25 and GO/NRL, which had ~3.1×10^{-4} Scm^{-1} and ~2.6×10^{-4} Scm^{-1}, respectively. The results obtained were 10^2 magnitudes higher than those of the pristine GO film in a previous work [22].

The slightly high conductivity for GO/RVNRL polymer nanocomposite is believed to be due to the homolytic process that occurred after irradiation of the latex particles [23]. The stable latex particles upon irradiation directly opened up the latex structure for further crosslinking with the incorporation of GO. Moreover, the defects of the GO/RVNRL polymer nanocomposite samples were higher than the other polymer nanocomposites, as indicated from the micro-Raman analysis. Therefore, several forms of defects, such as carboxylic and epoxide groups in the GO sheets, probably enhanced the electrical properties, as these defects are believed to act as an effective reactive site for the electron pathways [24]. High defect levels in the GO/RVNRL polymer nanocomposite were also accredited to the strong interaction between the GO dispersion and RVNRL matrix.

Another factor believed to assist the differences in the electrical conductivity improvement for the GO/RVNRL polymer nanocomposite was the presence of crosslinks in the latex itself. The RVNRL polymer contains the highest number of crosslinks due to the irradiation processes that introduced many free radicals in the structure [25]. This probably enhanced the crosslinking between GO sheets and the RVNRL polymer matrix. In addition, due to the double-stage fabrication of the GO/ENRL 25 polymer nanocomposite, the GO/RVNRL polymer nanocomposite samples produced via the one-step method had a more efficient and simple way in fabricating the nanocomposites.

Meanwhile, a slight improvement in the GO/ENRL 25 polymer nanocomposite, as compared with the GO/NRL polymer nanocomposite, confirmed that the GO sheets formed a better interconnection in the ENRL 25 matrix than the GO/NRL polymer nanocomposite. The electrical improvement is believed to be due to the associated epoxy group

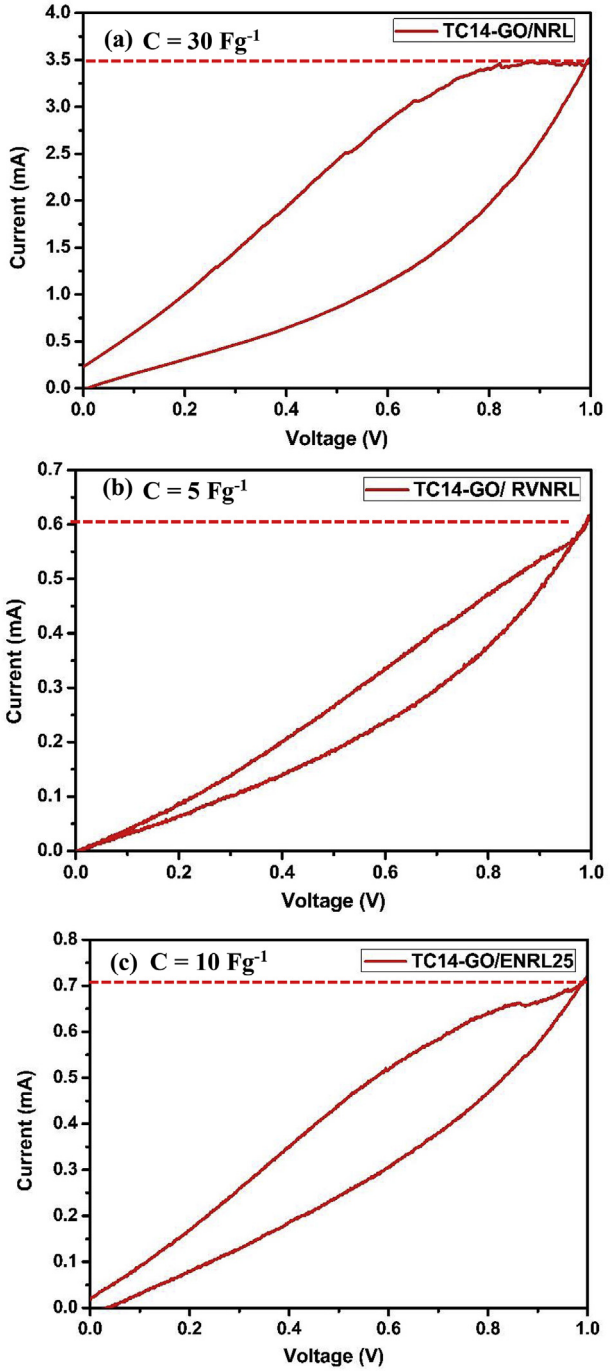

Fig. 3. *C–V* curves of the (a) GO/NRL, (b) GO/RVNRL, and (c) GO/ENRL 25 polymer nanocomposites.

in the structure of the ENRL 25 polymer, which increased the interaction and connection between the GO dispersions and ENRL 25 matrix. The increase in the interaction and connection is due to the fact that GO also possessed high aspect ratios and moderate conductivity, which helped in the formation of electrical conductive pathways by the GO sheets in the ENRL 25 matrix [26,27]. The data are tabulated in the supplementary material.

3.2. Cyclic voltammetry measurements

The *C–V* properties of the prepared nanocomposite samples were studied to investigate the capacitance performance of the polymer nanocomposite produced, as presented in Fig. 3. The *C–V* measurement of the polymer nanocomposite samples was carried out within a potential window of 0–1 V using a 1 M KOH solution. Generally, the addition of GO in the different types of NRL polymer nanocomposite enhanced the supercapacitor performance. The nanocomposite electrodes exhibited a leaf-like curve. The cyclic pattern was known to contribute to the enhancement of the charge-discharge process between the electrodes in the supercapacitor application. However, the cyclic behavior was distorted from a rectangular shape due to the densely packed GO layer used in the different types of RVNRL matrix. This might be explained as the electrolyte ions are kinetically limited from penetrating into the inner GO structure at a high scan rate [28].

The highest specific capacitance was presented by the GO/NRL polymer nanocomposite (30 Fg^{-1}), followed by the GO/ENRL 25 polymer nanocomposite (10 Fg^{-1}) and GO/RVNRL (5 Fg^{-1}). The difference in specific capacitance obtained was speculated not only due to the acceptable high conductivity ($\sim \times 10^{-4}$ Scm^{-1}) but also to the GO wrinkles distributed in the matrices, which ensured the formation of sufficient electric double layers [29]. The GO wrinkles' structures has increased the platform of the ion movement between the electrodes and electrolyte due to the insertion of many oxygen functional groups, thus improving its specific capacitance. This finding was consistent with the higher current response achieved by the GO/NRL polymer nanocomposite (~3.5 mA) than the GO/ENRL 25 (~0.72 mA) and GO/RVNRL polymer nanocomposites (~0.6 mA). The summarized results are presented in the supplementary material.

The lowest capacitance performance of the GO/RVNRL polymer nanocomposite was observed, which presumably resulted as part of the oxygen functional groups on the GO structure are unable to participate at a high scan rate [30]. In addition, the highest number of defects presented in the RVNRL matrix might restricted the penetration of ions in the electrodes. The crosslinks existing in the RVNRL matrix has promoted the higher interaction between the GO sheets and RVNRL matrix, thus reducing the wrinkle structures of GO in the nanocomposite, and leading to the low access of ion penetration in the electrode materials. This phenomenon has resulted to the lowest specific capacitance obtained for the GO/RVNRL polymer nanocomposite sample (C = 5 Fg^{-1}). Capacitance performance is actually applicable and reliable when considering that the electrodes were free from other carbon additives. The results hold a potential for the design of highly bendable and fast charge-discharge supercapacitor devices. In the following section, the structural properties of the nanocomposites produced are briefly explained to support the electrical conductivities and capacitance performance enhancement.

3.3. Surface morphology observations

The nanocomposite samples produced using different polymers, which include NRL, RVNRL, and ENRL 25 polymer nanocomposites were also prepared for structural characterizations. Prior to the fabrication of GO in the NRL polymers, the surface morphology analysis of pristine GO was observed through FESEM, as shown in the supplementary material. The typical wavy appearance of separated graphitic sheets was observed to presumably have occurred due to the successful oxidation process via the electrochemical exfoliation method.

Meanwhile, the FESEM images of GO/NRL, GO/RVNRL, and GO/ENRL 25 polymer nanocomposite samples are presented in Fig. 4. Fig. 4a reveals the formations of bumpy-like-particles of GO, which are unevenly distributed in the polymer nanocomposite. This is believed to be due to the high interaction of van der Waals for the GO itself therefore resulting in poor GO-NRL interaction as discussed in a previous study [31]. Big agglomerated GO particles were pulled out from the NRL interface, thus resulting in a slightly low electrical conductivity measured for the GO/NRL polymer nanocomposite ($\sigma = \sim 2.6 \times 10^{-4}$ Scm^{-1}).

Meanwhile, a fracture and few crack surfaces were observed in the GO/RVNRL polymer nanocomposite (pointed by red arrows in Fig. 4b.

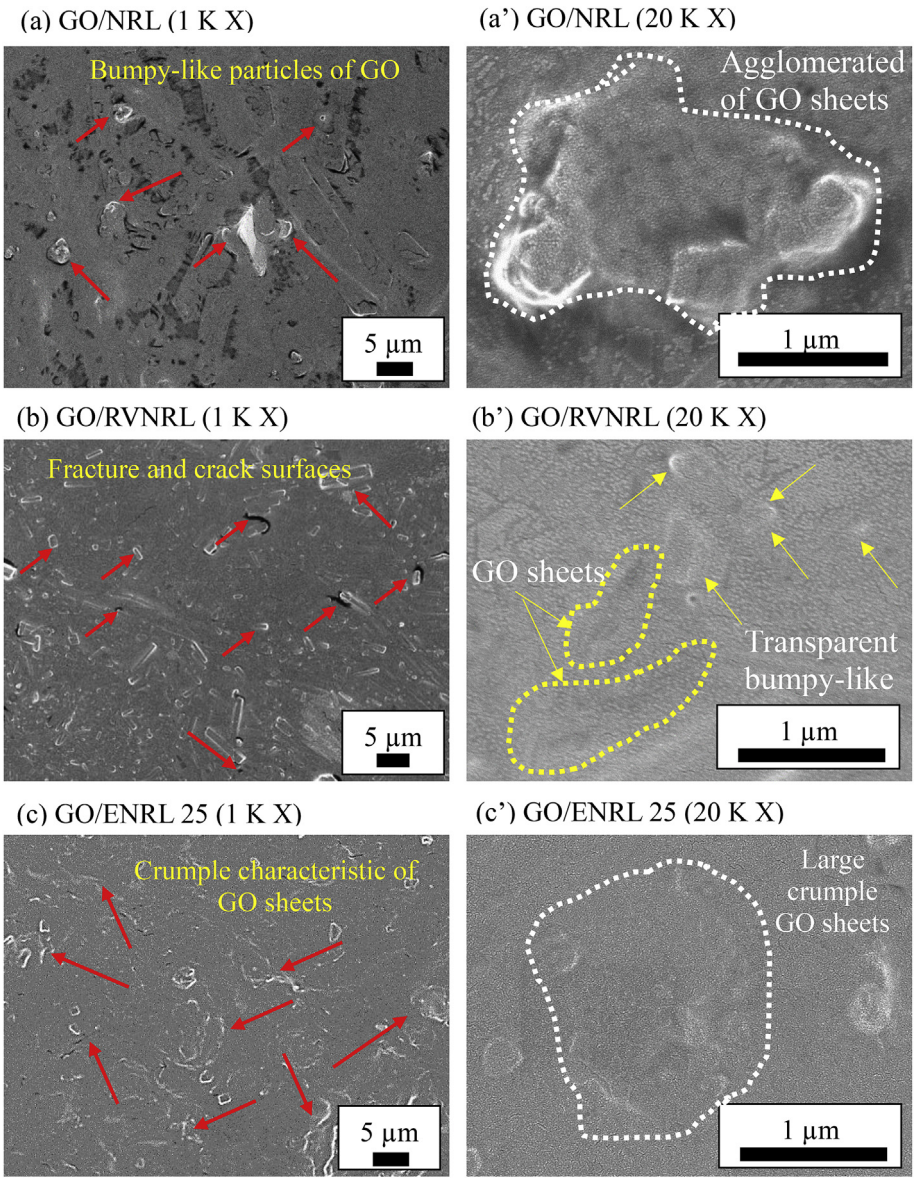

Fig. 4. FESEM images of the (a)-(a') GO/NRL, (b)-(b') GO/RVNRL, and (c)-(c') GO/ENRL 25 polymer nanocomposites.

In addition, the absence of rough bumpy-like GO particles was observed in a high-magnification image. These characteristic morphologies were considered responsible for the better interaction of linked-radiated chain with the GO surfaces [32]. For the GO/ENRL 25 polymer nanocomposite, the crumple characteristic of GO sheets was observed on the surface even in a high-magnification image. This may be due to the incomplete insertion of the polar group of epoxy into the interlayer spacing of the GO sheets, which resulted to the pull-out of GO layers from the polymer nanocomposite [33]. However, the GO/ENRL 25 polymer nanocomposite showed better interaction as compared with the GO/NRL polymer nanocomposite sample.

These results were supported by the EDX analysis presented in Fig. 5. The GO/NRL polymer nanocomposite has an oxygen and carbon contents of 36.95% and 54.08%, respectively. Meanwhile, the GO/RVNRL polymer shows the highest atomic percentage of carbon at 75.16%, indicating the successful intercalation and tight bond between the GO and RVNRL matrix. The GO/ENRL 25 polymer nanocomposite sample possesses a lower carbon percentage, estimated to be 55.04%, compared with the GO/RVNRL polymer nanocomposite samples. This finding justifies a significant weak interaction between the GO dispersions and the NRL and ENRL 25 polymers, as convincingly shown in the FESEM images.

The effects of GO synthesized in the different NRL polymers were further investigated via the optical micrographs observations, as shown in Fig. 6. Fig. 6 show the different magnifications of optical micrographs of GO dispersions in the different types of NRL matrices at a micrometer scale. Almost all polymer nanocomposite samples show a loosely pack of GO clusters (shown by arrows) distributed in the matrices. Such aggregate clusters were obviously seen throughout the NRL, RVNRL, and ENRL 25 matrices due to the strong van der Waals attraction between the GO sheets [34] as compared with the interactions between the GO and the NRL matrix [35].

Meanwhile, the island-like morphologies for GO/NRL and GO/RVNRL polymer nanocomposite samples were observed, as shown in high-magnification images (Fig. 6a'-b'). This might be attributed to the high compatibility of the hydrophobic GO sheets with the NRL and RVNRL matrices. However, the GO/RVNRL polymer nanocomposite shows fewer regions of island-like structures due to the higher interaction between the oxygen functional groups of the GO sheets and hydroxyl groups and free radicals in the RVNRL polymer matrix, thus yielding a homogeneous distribution and higher electrical conductivity.

As compared with the GO/ENRL 25 polymer nanocomposite, the

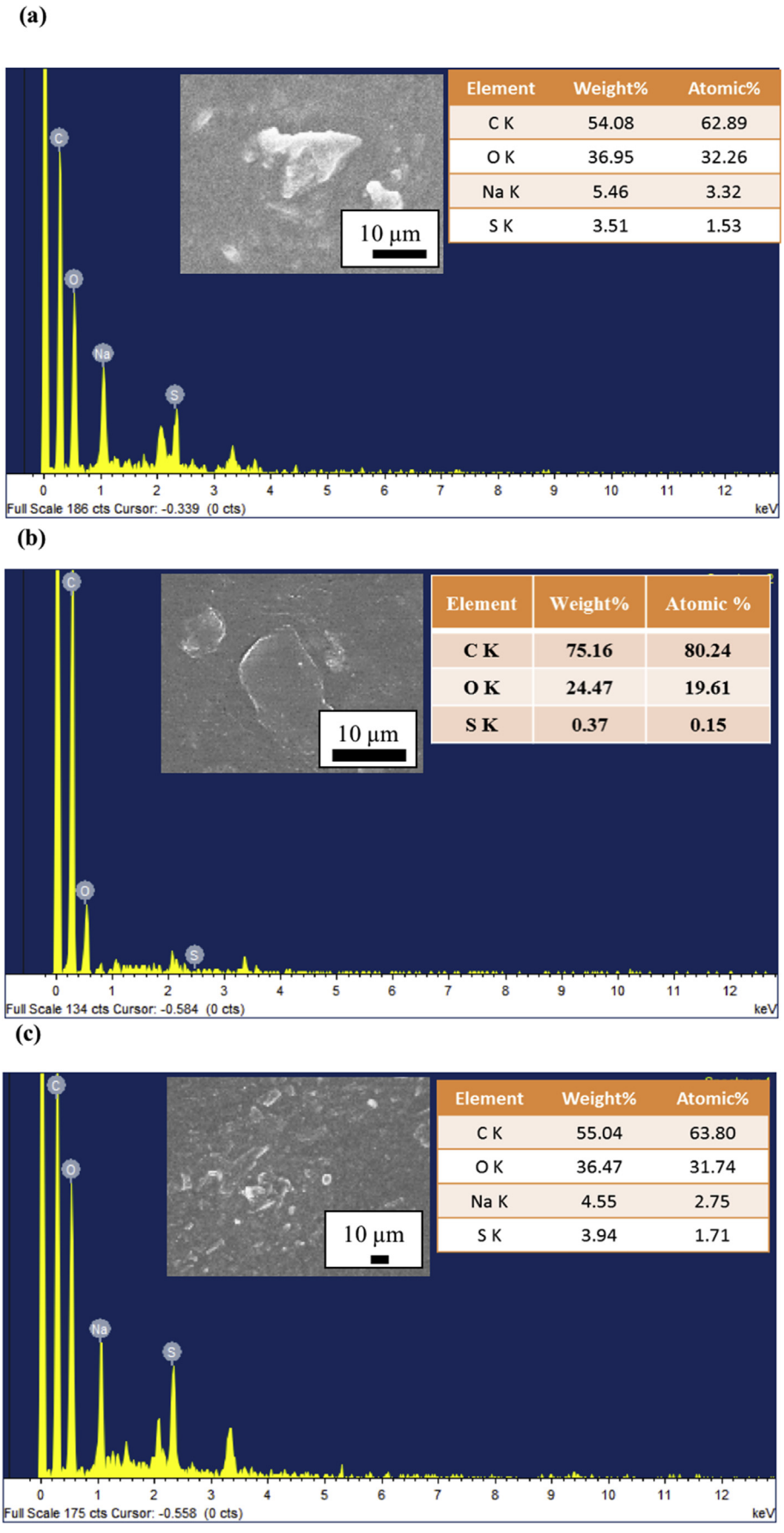

Fig. 5. EDX spectra of the (a) GO/NRL, (b) GO/RVNRL, and (c) GO/ENRL 25 polymer nanocomposites.

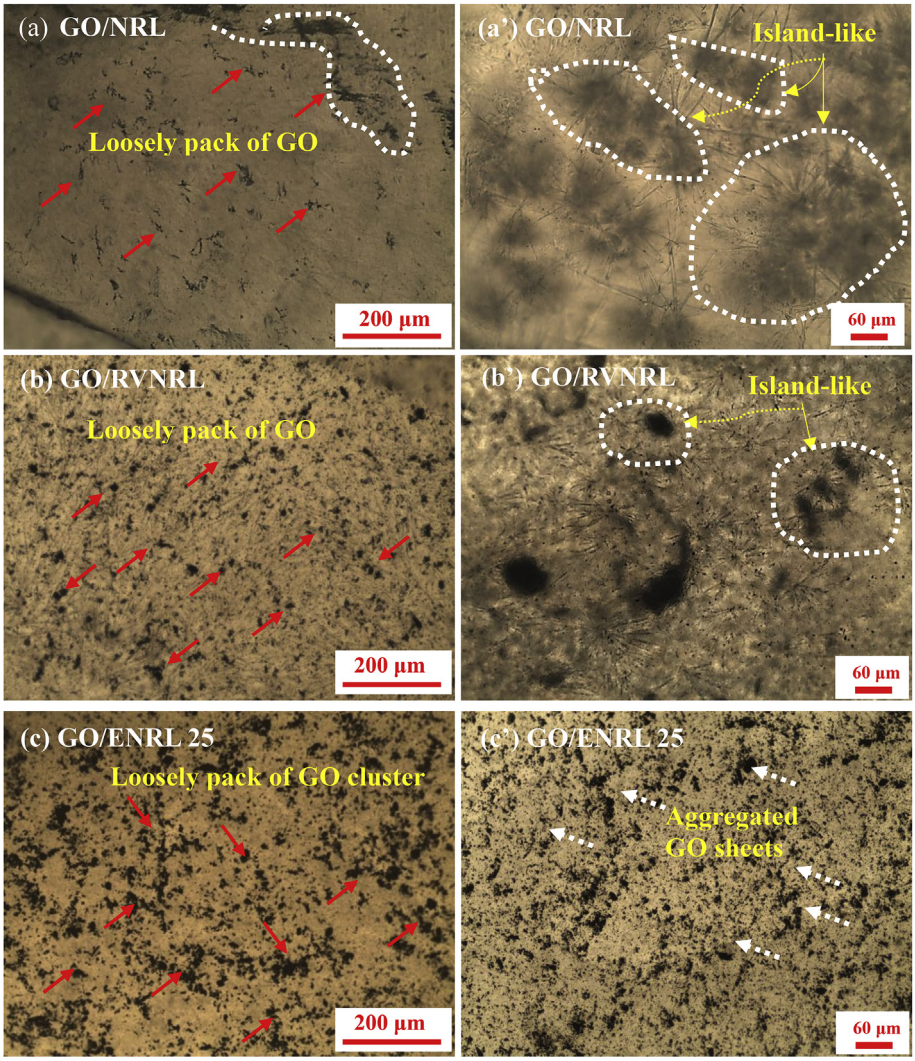

Fig. 6. OPM micrographs of the (a)-(a') GO/NRL, (b)-(b') GO/RVNRL, and (c)-(c') GO/ENRL 25 polymer nanocomposites.

nanocomposite sample shows more aggregated GO sheets, as shown in Fig. 6c, which is believed to be due to the low compatibility between the GO-assisted home-made TC14 surfactant and the epoxy groups in the ENRL 25 matrix. Thus, a high density of GO sheets was seen to be pulled out from the ENRL 25 matrix. The few aggregated GO clusters accumulated in a specific region in the polymer nanocomposite samples also contributed to the blurred images for the GO/NRL polymer nanocomposite due to the lowering intensity of light transmitting through the samples [36,37]. In comparison, the GO/RVNRL and GO/ENRL 25 polymer nanocomposites showed well-dispersed connected GO sheets throughout the RVNRL and ENRL 25 matrices. This might be the main reason for the better electrical conductivities of both samples, as compared with the GO/NRL polymer nanocomposites.

HRTEM was also employed to investigate the morphologies of the GO sheets in the nanocomposites. Fig. 7 reveal the dispersion level of GO sheets in three types of polymer matrices. In general, dark portions in the HRTEM images were observed in almost all nanocomposite samples, which implies that the aggregated GO sheets were due to the strong van der Waals interaction [34]. Meanwhile, the magnified images show that the distributed GO sheets were visible but almost transparent. This finding demonstrates that the GO sheets were well-distributed and the oxygen functional groups in the GO structures interacted with the hydroxyl groups in the NRL polymers.

The GO/NRL polymer nanocomposite shows a low exfoliated GO in the matrices with the appearance of a big cluster on the nanocomposite surface. This is probably due to the restacking behavior of the GO itself and the low covalent reaction between the GO and NRL matrix [34]. By contrast, uniformly attached GO particles are assisted by the TC14 surfactant on the surface of the GO/RVNRL polymer nanocomposite, which can be viewed by big and large exfoliated GO sheets (yellow dotted curve) and well-dispersed GO in the RVNRL matrix, as compared with the GO/NRL and GO/ENRL 25 polymer nanocomposites shown by small arrows and dotted curves. The high synergistic effect of the GO dispersions stabilized by triple-tails TC14 surfactant and RVNRL matrix contributed to the enhancement in the dispersion level in the polymer nanocomposite, leading to the fracture surface as observed in the FESEM images. The fracture surface observed for the GO/RVNRL polymer nanocomposite sample evidences a better interaction between the oxygen functional groups of the GO sheets and the hydroxyl groups and free radicals in the RVNRL matrix.

In comparison, the GO/ENRL 25 polymer nanocomposite shows a decrease in the cluster size of the GO and transparent sheets, as pointed by the arrows and dotted lines, as compared with the GO/NRL polymer nanocomposite. This was due to the improved compatibility and covalent reaction between the GO dispersions and the ENRL 25 matrix with the presence of epoxide end groups in the ENRL 25 matrix [38]. However, some large agglomerates of the GO sheet (dark region) in the ENRL 25 polymer matrix (pointed by red arrow and dotted curve) can still be seen on the matrix surface, thus producing non-uniform surfaces as compared with the GO/RVNRL polymer nanocomposite.

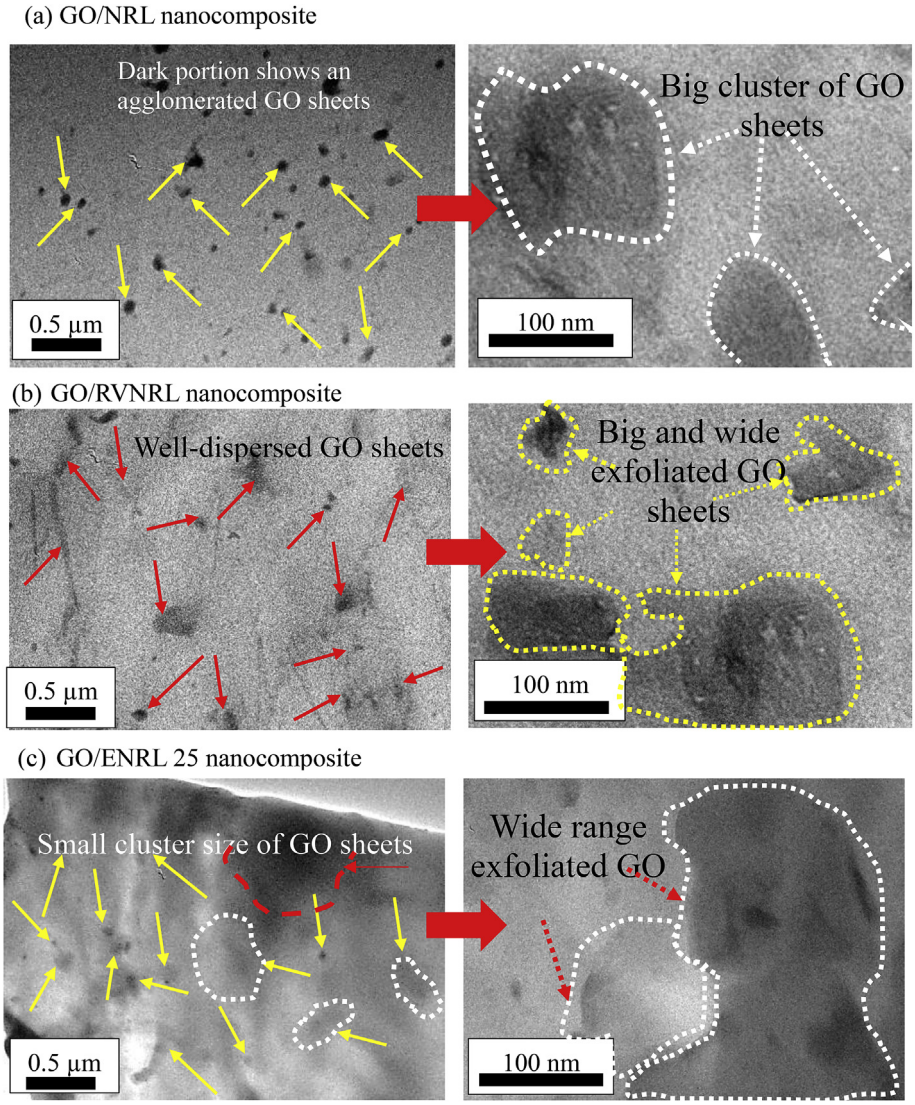

Fig. 7. HRTEM images of the (a) GO/NRL, (b) GO/RVNRL, and (c) GO/ENRL 25 polymer nanocomposites.

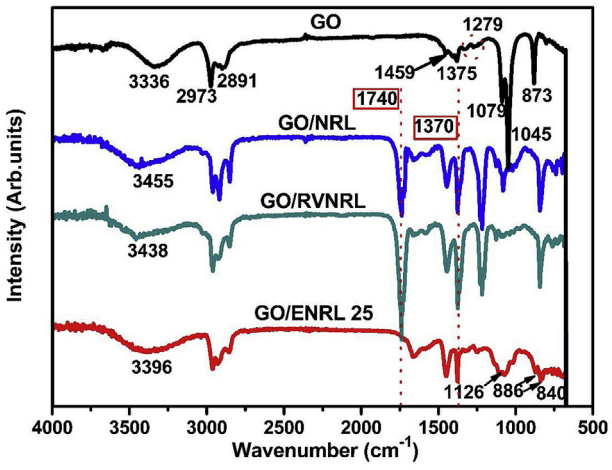

Fig. 8. FTIR analyses of the pristine GO, GO/NRL, GO/RVNRL, and GO/ENRL 25 polymer nanocomposites.

The interfacial interaction between the GO dispersions and NRL matrices was further investigated through the FTIR spectra, as shown in Fig. 8. Before the addition of GO dispersions in the polymer matrix, the FTIR spectrum of the GO showed several characteristics. Obviously, the broad peak at ~3336 cm^{-1} was assigned to the stretching of the –OH groups on the GO sheets [39]. The weak asymmetric and symmetric peaks appeared at ~2891 and 2973 cm^{-1}, respectively, indicating the vibrations of C–H groups from the surfactant molecules attached along the GO sheets [40]. In addition, the hexagonal carbon structures of C–C stretching in the aromatic ring could be detected through the existence of a weak peak at around ~1459 cm^{-1} [40]. Peaks at ~1279 and 1375 cm^{-1} were clearly observed, which may be attributed to the stretching vibration of the C–O and C–O–C groups, respectively [40]. Meanwhile, the sharp and intense peaks at ~1079, 1045, and 873 cm^{-1} unveiled the stretching vibrations of the carboxylic, epoxy, and carbonyl groups [39,41,42]. The FTIR results have confirmed the presence of various functional groups in the GO sheets.

In the case of the nanocomposite, the broad absorption bands at hydroxyl groups (O–H) and a strong peak around ~1370 cm^{-1}, which indicated the vibration of CH_3 in isoprene units [43], were observed in all nanocomposite samples (shown by the dotted lines). Meanwhile, a clear peak at around ~1740 cm^{-1}, which is characteristic of the carbonyl group of fatty acid ester of the linked phospholipids [43], was found in the GO/NRL and GO/RVNRL polymer nanocomposites but disappeared in the GO/ENRL 25 polymer nanocomposite, which confirmed the absence of phospholipids linked to the NRL polymer chain

(shown by the dotted lines). The presence of the proteins and phospholipid components in the NRL and RVNRL matrices were believed to enhance the structural properties of the polymers and promote rubber crystallization, which might later give the distinctive properties of the GO/NRL nanocomposite [44,45]. The obvious and highest intense peak at 1740 cm^{-1} in the GO/RVNRL polymer nanocomposite as compared with GO/NRL polymer nanocomposite confirmed an improved homogeneity of the nanocomposite and better interaction as proved in the FESEM and HRTEM analyses.

In addition, the GO/ENRL 25 polymer nanocomposite spectrum shows a slightly different intensity pattern. The GO/ENRL 25 polymer nanocomposite sample has a weak peak around ~880 cm^{-1}, which was attributed to the bending vibration of CH_2 in the –C═CH_2 [43] (pointed by the small arrows). Weak absorption bands were observed around ~1126 and 840 cm^{-1}, which was attributed to the vibrations of the epoxy groups [46] and the cis-alkene group [47] (pointed by the small arrows). These groups appeared due to the epoxide structure of the ENRL 25 polymer and ring-opening reactions in the formation of the GO/ENRL 25 polymer nanocomposite [48].

As mentioned before, the absorption band of GO around 3336 cm^{-1} was red-shifted in the polymer nanocomposite samples. This was attributed to a new formation of the hydrogen bonds between the epoxy (in ENRL 25 polymer), hydroxyl (in other polymers), and oxygeneous groups of the GO sheets [49]. However, the GO/RVNRL polymer nanocomposite shows a higher red-shift with the lowest intensity at the –OH groups, calculated around 119 cm^{-1}, as compared with the GO/NRL and GO/ENRL 25 polymer nanocomposites with 102 and 60 cm^{-1}, respectively. Therefore, the peak at ~3300 cm^{-1} in the GO/RVNRL polymer nanocomposite sample confirmed the effective interaction between the GO and RVNRL matrix, which subsequently reduced the –OH intensity. Again, the GO/RVNRL polymer nanocomposite confirmed the structural properties and effective interaction at ~1740 cm^{-1} and red-shift at ~3336 cm^{-1}.

To observe whether the stacking GO synthesis was ordered, micro-Raman spectroscopy was carried out. The micro-Raman spectra of pristine GO and polymer nanocomposite samples are given in Fig. 9. The pristine GO has an I_D/I_G ratio of 0.82, which indicated a typical quality of GO produced via the electrochemical exfoliation method. The characteristic peaks of GO at 1347.0–1364.5 (D-peak) and 1577.4–1665.2 cm^{-1} (G-peak) were clearly observed in all nanocomposite samples. Generally, a higher D-peak detected from the micro-Raman spectra for the NRL-based polymers were due to the highly amorphous nature of NRL-based polymers, as compared with the other polymers [50].

By focusing on the micro-Raman spectra of GO/NRL and GO/ENRL 25 polymer nanocomposite samples, shifted peaks and low intensity were detected around ~1347.0–1352.9 and 1577.4–1581.2 cm^{-1}. The low intensity of GO in the GO/NRL polymer nanocomposite synthesized via the one-step method was suggested due to the low amount of agglomerated GO diffused between the rubber matrices. The red shift from 1595.5 cm^{-1} (pristine GO) to 1577.4 cm^{-1} for the GO/ENRL 25 polymer nanocomposite shows the enhanced networking of hexagonal of atom carbon GO due to the interaction created between the epoxy and hydroxyl groups, which is proven by the appearances of a uniform distribution of wrinkled GO sheets over the ENRL 25 matrix, as compared with the GO/NRL polymer nanocomposite in the FESEM image. The results can be further confirmed by the slightly higher I_D/I_G ratio of GO/ENRL 25 polymer nanocomposite, which was 1.00, as compared to the GO/NRL polymer nanocomposite (I_D/I_G = 0.95), which is believed to be due to the good linkage that was promoted by the epoxy group in the ENRL 25 matrix. These results were supported by the OPM, FESEM, and HRTEM analyses.

However, the distribution of GO in the RVNRL matrix has the highest I_D/I_G ratio of 1.08, as compared with the GO/NRL and GO/ENRL 25 polymer nanocomposite samples, which were 0.95 and 1.00, respectively. This finding confirmed that the GO dispersions stabilized by the home-made surfactant, TC14 and the RVNRL polymer, were highly self-linked during the electrochemical exfoliation method which contributed to the higher distortion in aromatic structures. Furthermore, the G-peak blue-shifted from 1595.5 cm^{-1} (pristine GO) to the longer wavelength of 1665.2 cm^{-1} in the GO/RVNRL polymer nanocomposite sample proved that a low number of stacked GO sheets might appear in the nanocomposite due to the higher interaction between the oxygen functional groups of the GO sheets and the RVNRL matrix, thus leading to a higher shifted peak of approximately 69.7 cm^{-1}. In comparison, the GO/NRL and GO/ENRL 25 polymer nanocomposite samples show a red-shift at approximately 14.3 and 18.1 cm^{-1}, respectively, which was expected due to the increased number of agglomerated GO sheets in the matrices. The result obtained for the GO/RVNRL polymer nanocomposite supports the improvement in the electrical conductivity and homogeneous distribution of the sample. The summaries of the micro-Raman analyses are tabulated in the supplementary material.

In a further structural investigation, the XRD spectroscopy was employed to confirm the existence and crystallinity of the GO in the nanocomposite samples. Based on the XRD pattern given in Fig. 10, the pristine GO sample shows a typical peak of GO at 2θ value of ~10.27° assigned to (002) planes. After the addition of the NRL polymer, an obvious peak at ~17.58° in the GO/NRL nanocomposite arises due to some re-aggregation of intercalated layers of the GO sheets [51]. Meanwhile, the absence of a strong peak at ~17.58° for the GO/RVNRL

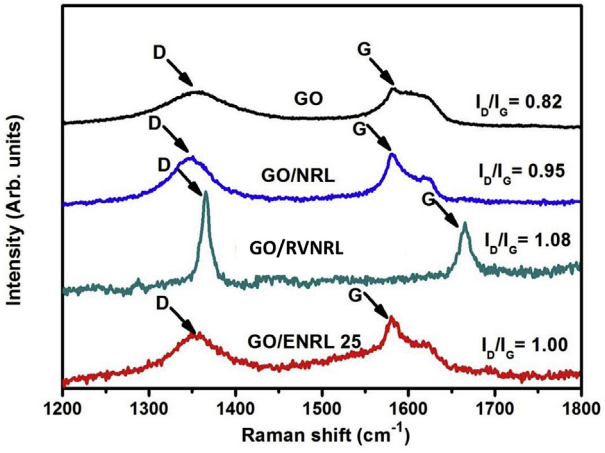

Fig. 9. Micro-Raman spectra of the pristine GO, GO/NRL, GO/RVNRL, and GO/ENRL 25 polymer nanocomposites.

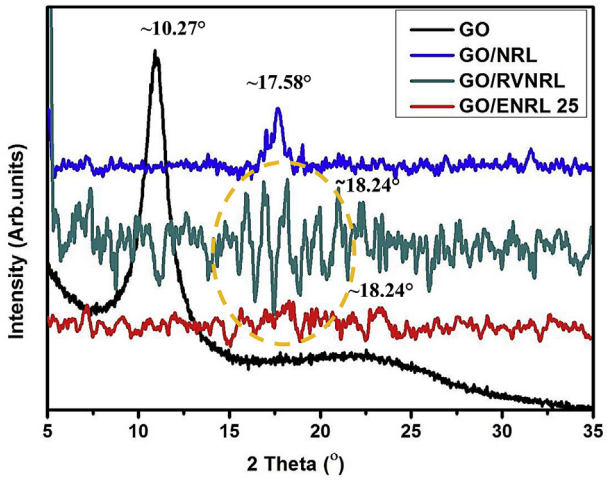

Fig. 10. XRD spectra of the pristine GO, GO/NRL, GO/RVNRL and GO/ENRL 25 polymer nanocomposites.

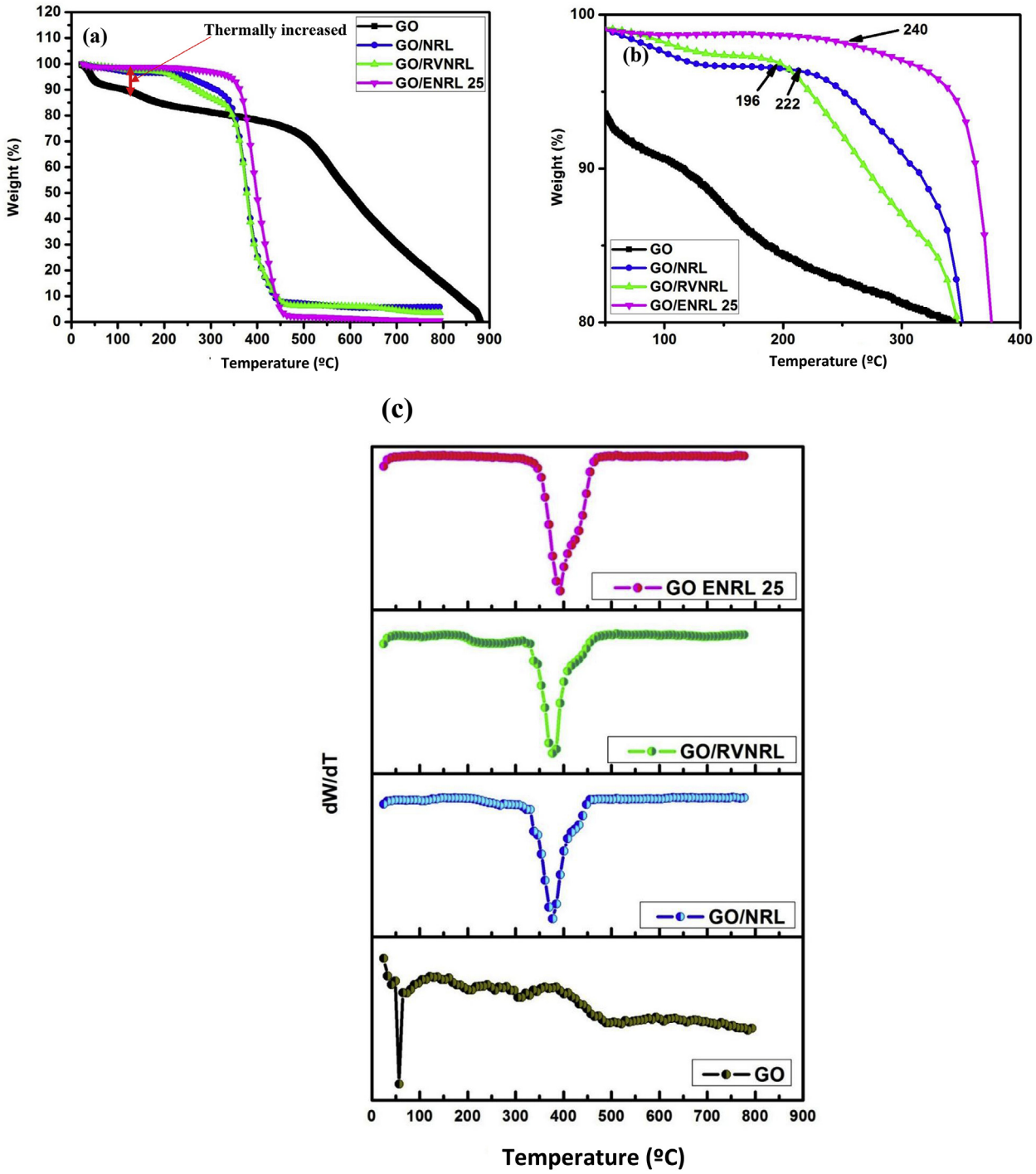

Fig. 11. TGA and (c) DTGA curves of the GO/NRL, GO/RVNRL, GO/ENRL 25 polymer nanocomposites.

and GO/ENRL 25 nanocomposites proves the better exfoliation of GO sheets in the matrices. However, the obvious broad and intense peak observed at ~18.24° for the GO/RVNRL polymer nanocomposite suggests the formation of a high interaction between the GO sheets and the RVNRL matrix thus leading to more homogeneous nanocomposites as compared with the GO/ENRL 25 and GO/NRL nanocomposites.

TGA was utilized to examine the stability of GO-filled polymer nanocomposite samples. The degradation temperatures of pristine GO, GO/NRL, GO/RVNRL, and GO/ENRL 25 polymer nanocomposites are presented by the TGA curves in Fig. 11a. Before the incorporation with NRL polymers, the pristine GO shows the gradual decrease of degradation temperature due to the presence of unstable functional groups on the GO structures [52]. Meanwhile, the TGA curves for the nanocomposite samples show an obvious increase in the thermal stability, as shown by the red line, as compared with the pristine GO itself. The nanocomposite samples show two clearer stages of decomposition in the range of ~200–450 °C which were attributed to the percentage of water and ammonia decomposition from the GO and polymers [53,54], the decomposition of polymer backbone [20,21,55] and low boiling point of rubber chemicals [56]. Due to the naturally depolymerized NRL under certain heat conditions, the polymer part was degraded into isoprene, dipentene, and p-menthene, as reported in a previous study [57].

For the nanocomposite samples, the GO/RVNRL polymer

nanocomposite shows an onset decomposition around ~196 °C, followed by the GO/NRL (~222 °C) and GO/ENRL 25 (~240 °C) polymer nanocomposites, as shown in Fig. 11 (b). The early decomposition of the GO/RVNRL polymer nanocomposite was due to the strong interfacial bonding effect leading to the increase in the covalent bonding and gamma crosslinking interaction between the GO and the RVNRL matrix, as compared with the GO/NRL and GO/ENRL 25 polymer nanocomposite samples [32,58,59]. In addition, the free radicals consist of the RVNRL structures and the existence of double bonds in the RVNRL and NRL polymer backbones were susceptible to degradation first, as compared with the ENRL 25 polymer [56,60].

Moreover, the onset degradation at around ~200–350 °C was attributed to the decomposition of oxygen functional groups, such as C=O, C–O–C, and –OH, from the GO dispersion [61]. The weight loss by the GO/RVNRL polymer nanocomposite in this temperature region was calculated as 14 *wt*%, as compared with GO/NRL (16 *wt*%) and GO/ENRL 25 (20 *wt*%). For the GO/RVNRL polymer nanocomposite, the amounts of oxygen groups were 36.95 *wt*%, according to the elemental analysis, and the quantity of decomposed oxygen was approximately 14 *wt*%, according to TGA analysis. The small amount of the weight loss observed was related to the non-full decomposition of oxygen groups due to the high interaction between the GO sheets and the free radicals of the RVNRL matrix. As compared with the GO/ENRL 25 polymer nanocomposite, the significantly large amount (20 *wt*%) of weight loss in this temperature region indicates that the GO/ENRL 25 polymer nanocomposite contains much water due to the incompatible mixing between the TC14-GO with the ENRL 25 matrix, as proven by the difficulty to mix via a one-step method of electrochemical exfoliation, thus producing an easy degradation step at this stage.

The nanocomposite samples were observed to burn up at above 400 °C with a residual weight loss of 7% for the GO/NRL and GO/RVNRL polymer nanocomposites and 3% for the GO/ENRL 25 polymer nanocomposite. The residual weight loss was believed to be due to the behavior of the GO itself and other non-volatile compounds [56,60]. Meanwhile, the pristine GO shows a slow decomposition up to 900 °C. The slightly lower degradation temperature of the GO/RVNRL polymer nanocomposite was also probably due to the effective diffusion of GO dispersions into the RVNRL matrix. The result was in a good agreement with the FESEM, HRTEM, FTIR and micro-Raman analyses, as previously discussed.

Fig. 11b shows the DTGA curves of pristine GO, GO/NRL, GO/RVNRL and GO/ENRL 25 polymer nanocomposites. Pristine GO shows a clearer single-step degradation in the range of 0–100 °C. Meanwhile, the double-step degradation was observed in the nanocomposite samples as the obvious peaks were located at 380 °C, 376 °C, and 397°C, whereas the shoulder peaks were located at 397 °C, 388 °C, and 426 °C for the GO/NRL, GO/RVNRL, and GO/ENRL 25 polymer nanocomposites, respectively. The results were attributed to the breaking of the main chains of polymers in the nanocomposite samples [60]. The slightly different degradation steps in the nanocomposite samples were related to the chemical reaction between the oxygenic functional groups from the GO, hydroxyl, and epoxy groups and the free radicals from the polymers, leading to the formation of rubber-filler interaction between the GO sheets and the NRL polymers [49,60]. This result shows that the high interaction of the GO/RVNRL polymer nanocomposite presents a better thermal stability than the GO/NRL polymer nanocomposite. The highly crosslinked RVNRL matrix improved the interconnection between the GO particles, thus leading to electrical and structural enhancement.

Meanwhile, the ENRL 25 nanocomposite filled with GO sheets presented the highest thermal stability, which showed that the presence of the epoxy group in the matrix improved its thermal behavior and electrical properties, as compared with the pure NRL matrix-based nanocomposite. However, due to the cumbersome double-stage preparation, the GO/ENRL 25 polymer nanocomposite as compared with the GO/RVNRL polymer nanocomposite was seen as inefficient electrode materials for scalable productions. The details of the decomposition temperatures are summarized in the supplementary material.

These results illustrate how differences in compatibility between the GO and matrix can affect electrical, capacitance, and structural properties. The starting point for the production of each type of nanocomposite was a kinetically stable aqueous suspension of the nanofiller, which was mixed with NRL and subsequently co-coagulated. However, the surface chemistry mismatch between GO dispersions and NRL polymers may have driven some agglomeration of GO via a two-step method. Therefore, some efforts to reduce GO were taken. This attempt may give further information regarding the important role of GO in enhancing the electrical, and structural properties and its capacitance performance.

4. Conclusions

In summary, the fabrications of GO/NRL polymer nanocomposites in this study were prepared by two approaches, namely, one- and two-step methods of electrochemical exfoliation. Significant differences in the GO/NRL polymer nanocomposite morphologies were found using the two methods, resulting from the differences in polymer groups introduced. By using the one-step method, the GO/RVNRL nanocomposite demonstrated better uniformity as compared with the GO/NRL polymer nanocomposite sample. The one-step method adopted was seen as a simple route for fabricating GO/RVNRL polymer nanocomposites in comparison with GO/ENRL 25 polymer fabrication via the two-step method. The homogeneous dispersion of the GO/RVNRL polymer nanocomposites obtained led to the improvement in the electrical conductivity, which was $\sim 8.6 \times 10^{-4}$ Scm^{-1}, as compared with the GO/ENRL 25 ($\sim 3.1 \times 10^{-4}$ Scm^{-1}) and GO/NRL ($\sim 2.6 \times 10^{-4}$ Scm^{-1}) polymer nanocomposites. In addition, the GO/RVNRL polymer nanocomposites electrodes showed acceptable specific capacitance (5 Fg^{-1}). The use of one- and two-step methods to fabricate the nanocomposites paves the way for the greener and low cost processing method.

Declaration of competing interest

The authors declare that they have no known competing financial interests or personal relationships that could have appeared to influence the work reported in this paper.

Acknowledgements

The authors would like to acknowledge Short Term Grant, Universiti Sains Malaysia (304/PFIZIK/6315241) for the financial support. The authors want to thank Nano-Optoelectronics Research and Technology Lab (USM) and Universiti Pendidikan Sultan Idris (UPSI) for their facilities support. Authors are thankful to Malaysian Rubber Board industry for latex supplied.

Appendix A. Supplementary data

Supplementary data to this article can be found online at https://doi.org/10.1016/j.ceramint.2019.11.005.

Author contributions

MD Nurhafizah: 65% in conception, experimental design, carrying out measurement and manuscript composition.

AA Aziz: 5% in carrying out measurement.

AB Suriani: 15% in experimental design.

A Mohamed: 10% in conception.

T Soga: 5% in manuscript composition and proofreading.

References

[1] M.A. Lopez Manchado, B. Herrero, M. Aroro, Preparation and characterization of organoclay nanocomposites based on natural rubber, Polym. Int. 52 (7) (2003) 1070–1077.

[2] D. Salimi, S.N. Khorasani, M.R. Abadchi, S.J. Veshare, Optimization of physic-mechanical properties of silicate-filled NR/SBR compounds, Adv. Polym. Technol. 28 (4) (2009) 224–232.

[3] K. Ariga, J. Li, J. Fei, Q. Ji, J.P. Hill, Nanoarchitectonics for dynamic functional materials from atomic-/molecular-level manipulation to macroscopic action, Adv. Mater. 28 (2016) 1251–1286.

[4] A.R. Marlinda, B.T. Goh, H.K. Nurul, A.W. Fadilah, Z.C. Zaira, S. Suresh, C. Narong, R.J. Mohd, Effect of graphene infusion on morphology and performance of natural rubber latex/graphene composites, J. Mater. Sci. Mater. Electron. 30 (2019) 12888–12894.

[5] V.V. Rajan, W.K. Dierkes, R. Joseph, J.W.M. Noordermeer, Science and technology of rubber reclamation with special attention to NR-based waste latex products, Prog. Polym. Sci. 31 (9) (2006) 811–834.

[6] A.B. Suriani, M.D. Nurhafizah, A. Mohamed, A.K. Masrom, M.H. Mamat, M.F. Malek, M.K. Ahmad, M.S. Rosmi, M. Tanemura, Electrical enhancement of radiation-vulcanized natural rubber latex added with reduced graphene oxide additives for supercapacitor electrodes, J. Mater. Sci. 52 (2017) 6611–6622.

[7] Y. Li, Q. Wang, T. Wang, G. Pan, Preparation and tribological properties of graphene oxide/nitrile rubber nanocomposites, J. Mater. Sci. 47 (2012) 730–738.

[8] D.K. Chouhan, S.K. Rath, A. Kumar, P. Alegaonkar, S. Kumar, G. Harikrishnan, T.U. Patro, Structure-reinforcement correlation and chain dynamics in graphene oxide and laponite-filled epoxy nanocomposites, J. Mater. Sci. 50 (2015) 7458–7472.

[9] P.J. Teng, F.L. Shyu, Field-modulated electronic specific heat of armchair graphene nanoribbons, Physica E Low Dimens. Syst. 115 (2020) 113660.

[10] Q. Yan, Q. Liu, J. Wang, A simple and fast microwave assisted approach for the reduction of graphene oxide, Ceram. Int. 42 (2) (2016) 3007–3013.

[11] K. Hu, D.D. Kulkarni, I. Choi, V.V. Tsukruk, Graphene- polymer nanocomposites for structural and functional applications, Prog. Polym. Sci. 39 (11) (2014) 1934–1972.

[12] H. Li, X. Han, S.C. Anthony, M.R. Apparao, K. Goutam, Investigation of carrier density and mobility variations in graphene caused by surface adsorbates, Physica E Low Dimens. Syst. 107 (2019) 96–100.

[13] S. Stephen, S. Ochigbo Adriaan, W. Luyt Walter, Latex derived blends of poly (vinyl acetate) and natural rubber: thermal and mechanical properties, J. Mater. Sci. 44 (2009) 3248–3254.

[14] M. Hernandez, M.M. Bernal, R. Verdejo, T.A. Ezquerra, M.A. Lo'pez- Manchado, Overall performance of natural rubber/graphene nanocomposites, Compos. Sci. Technol. 73 (2012) 40–46.

[15] Y. Li, Q. Wang, T. Wang, G. Pan, Preparation and tribological properties of graphene oxide/nitrile rubber nanocomposites, J. Mater. Sci. 47 (2012) 730–738.

[16] W.S. Ma, L. Wu, F. Yang, S.F. Wang, Non-covalently modified reduced graphene oxide/polyurethane nanocomposites with good mechanical and thermal properties, J. Mater. Sci. 49 (2014) 562–571.

[17] G. Hatui, A. Malas, P. Bhattacharya, S. Dhibar, M.K. Kundu, C.K. Das, Effect of expanded graphite and PEI-co-Silicon Rubber on the thermo mechanical, morphological as well as rheological properties of in situ composites based on poly (ether imide) and liquid crystalline polymer, J. Alloy. Comp. 619 (2015) 709–718.

[18] C.-C. Teng, C.-C.M. Ma, C.-H. Lu, S.-Y. Yang, S.-H. Lee, M.-C. Hsiao, M.-Y. Yen, K.C. Chiou, T.M. Lee, Thermal conductivity and structure of non-covalent functionalized graphene/epoxy composites, Carbon 49 (15) (2011) 5107–5116.

[19] T.L.B. Sharmila, J.V. Antony, M.P. Jayakrishnan, P.M.S. Beegum, E. T, Thachil Mechanical, thermal and dielectric properties of hybrid composites of epoxy and reduced graphene oxide/iron oxide, Mater. Des. 90 (2016) 66–75.

[20] A.B. Suriani, M.D. Nurhafizah, A. Mohamed, I. Zainol, A.K. Masrom, A facile one-step method for graphene oxide/natural rubber latex nanocomposite production for supercapacitor applications, Mater. Lett. 161 (2015) 665–668.

[21] A.B. Suriani, M.D. Nurhafizah, A. Mohamed, A.K. Masrom, V. Sahajwalla, R.K. Joshi, Highly conductive electrodes of graphene oxide/natural rubber latex-based electrodes by using a hyper-branched surfactant, Mater. Des. 99 (2016) 174–181.

[22] J. Gao, F. Liu, Y. Liu, N. Ma, Z. Wang, X. Zhang, Environment-friendly method to produce graphene that employs vitamin C and amino acid, Chem. Mater. 22 (7) (2010) 2213–2218.

[23] C.T. Ratnam, M. Nasir, A. Baharin, K. Zaman, Electron beam irradiation of epoxidized natural rubber, Nucl. Instrum. Methods B 171 (4) (2000) 455–464.

[24] M. Ghislandi, E. Tkalya, A. Alekseev, C. Koning, G. De With, Electrical conductive behavior of polymer composites prepared with aqueous graphene dispersions, Appl. Mater. Today 1 (2) (2015) 88–94.

[25] J.A. Brydson, Rubber Chemistry, Applied Science Publishers, 1978.

[26] P.L. Teh, Z.A.M. Ishak, A.S. Hashim, J. Karger-Kocsis, U.S. Ishiaku, Effects of epoxidized natural rubber as a compatibilizer in melt compounded natural rubber/organoclay nanocomposites, Eur. Polym. J. 40 (11) (2004) 2513–2521.

[27] J. Li, P.C. Ma, W.S. Chow, C.K. To, B.Z. Tang, J.K. Kim, Correlations between percolation threshold, dispersion state, and aspect ratio of carbon nanotubes, Adv. Funct. Mater. 17 (16) (2007) 3207–3215.

[28] K. Zhang, L. Mao, L.L. Zhang, H.S.O. Chan, X.S. Zhao, J. Wu, Surfactant-intercalated, chemically reduced graphene oxide for high performance supercapacitor electrodes, J. Mater. Chem. 21 (20) (2011) 7302–7307.

[29] J. Yan, J. Liu, Z. Fan, T. Wei, L. Zhang, High-performance supercapacitor electrodes based on highly corrugated graphene sheets, Carbon 50 (6) (2012) 2179–2188.

[30] Z. Lei, L. Lu, X.S. Zhao, The electrocapacitive properties of graphene oxide reduced by urea, Energy Environ. Sci. 5 (4) (2012) 6391–6399.

[31] M. Fang, Z. Zhang, J. Li, H. Zhang, H. Lu, Y. Yang, Constructing hierarchically structured interphases for strong and tough epoxy nanocomposites by amine-rich graphene surfaces, J. Mater. Chem. 20 (43) (2010) 9635–9643.

[32] K. Makuuchi, An Introduction to Radiation Vulcanization of Natural Rubber-Latex, Bangkok: T.R.I. Global Co, 2003.

[33] Z. Tang, L. Zhang, W. Feng, B. Guo, F. Liu, D. Jia, Rational design of graphene surface chemistry for high-performance rubber/graphene composites, Macromolecules 47 (24) (2014) 8663–8673.

[34] L. Yue, G. Pircheraghi, S.A. Monemian, I. Manas-Zloczower, Epoxy composites with carbon nanotubes and graphene nanoplatelets: dispersion and synergy effects, Carbon 78 (2014) 268–278.

[35] H.C. Schniepp, J.-L. Li, M.J. McAllister, H. Sai, M. Herrera-Alonso, D.H. Adamson, R.K. Prudhomme, R. Car, D.A. Saville, I.A. Aksay, Functionalized single graphene sheets derived from splitting graphite oxide, J. Phys. Chem. B 110 (17) (2006) 8535–8539.

[36] Z. Xu, C. Gao, Aqueous liquid crystals of graphene oxide, ACS Nano 5 (4) (2011) 2908–2915.

[37] S. Yaragalla, B. Sindam, J. Abraham, K.C.N. Raju, S. Thomas, Fabrication of graphite-graphene-ionic liquid modified carbon nanotubes filled natural rubber thin films for microwave and energy storage applications, J. Polym. Res. 22 (7) (2015) 1–10.

[38] Y.-J. Wan, L.-X. Gong, L.-C. Tang, L.-B. Wu, J.-X. Jiang, Mechanical properties of epoxy composites filled with silane-functionalized graphene oxide, Compos A: Appl. Sci. Manufac. 64 (2014) 79–89.

[39] H. Lian, S. Li, K. Liu, L. Xu, K. Wang, Study on modified graphene/butyl rubber nanocomposites. I. Preparation and characterization, Polym. Eng. Sci. 51 (11) (2011) 2254–2260.

[40] C.-H. Chuang, C.-Y. Su, K.-T. Hsu, C.H. Chen, C.-H. Huang, C.-W. Chu, W.-R. Liu, A green, simple and cost-effective approach to synthesize high quality graphene by electrochemical exfoliation via process optimization, RSC Adv. 5 (67) (2015) 54762–54768.

[41] J. Luo, Y. Chen, Q. Ma, R. Liu, X. Liu, Layer-by-layer self-assembled hybrid multilayer films based on poly (sodium 4-styrenesulfonate) stabilized graphene with polyaniline and their electrochemical sensing properties, RSC Adv. 3 (39) (2013) 17866–17873.

[42] H.-L. Guo, X.-F. Wang, Q.-Y. Qian, F.-B. Wang, X.-H. Xia, A green approach to the synthesis of graphene nanosheets, ACS Nano 3 (9) (2009) 2653–2659.

[43] H.H. Le, S. Abhijeet, S. Illisch, J. Klehm, S. Henning, M. Beiner, et al., The role of linked phospholipids in the rubber-filler interaction in carbon nanotube (CNT) filled natural rubber (NR) composites, Polymers 55 (18) (2014) 4738–4747.

[44] W. Pichayakorn, J. Suksaeree, P. Boonme, W. Taweepreda, G.C. Ritthidej, Preparation of deproteinized natural rubber latex and properties of films formed by itself and several adhesive polymer blends, Ind. Eng. Chem. Res. 51 (41) (2012) 13393–13404.

[45] I. Cacciotti, J.N. House, C. Mazzuca, M. Valentini, F. Madau, A. Palleschi, P. Straffi, F. Nanni, Neat and GNPs loaded natural rubber fibers by electrospinning: manufacturing and characterization, Mater. Des. 88 (2015) 1109–1118.

[46] M. Ochi, Y. Shimizu, Y. Nakanishi, Y. Murata, Effect of the network structure on thermal and mechanical properties of mesogenic epoxy resin cured with aromatic amine, J. Polym. Sci. B 35 (2) (1997) 397–405.

[47] N.V. Bac, L. Terlemezyan, M. Mihailov, Oxidation of natural rubber and its derivatives prepared by epoxidation and subsequent hydrobromination, Eur. Polym. J. 26 (10) (1990) 1055–1060.

[48] H. Zhou, Y. Sun, G. Li, S. Chen, Y. Lu, Interfacial assembly and electrochemical properties of nafion-modified-graphene/polyaniline hollow spheres, Polymers 55 (17) (2014) 4459–4467.

[49] X. She, C. He, Z. Peng, L. Kong, Molecular-level dispersion of graphene into epoxidized natural rubber: morphology, interfacial interaction and mechanical reinforcement, Polymers 55 (26) (2014) 6803–6810.

[50] J. Wu, G. Huang, H. Li, S. Wu, Y. Liu, J. Zheng, Enhanced mechanical and gas barrier properties of rubber nanocomposites with surface functionalized graphene oxide at low content, Polymers 54 (7) (2013) 1930–1937.

[51] R. Rajasekar, K. Pal, G. Heinrich, A. Das, C.K. Das, Development of nitrile butadiene rubber-nanoclay composites with epoxidized natural rubber as compatibilizer, Mater. Des. 30 (9) (2009) 3839–3845.

[52] A. Malas, P. Pal, C.K. Das, Effect of expanded graphite and modified graphite flakes on the physical and thermo-mechanical properties of styrene butadiene rubber/polybutadiene rubber (SBR/BR) blends, Mater. Des. 55 (2014) 664–673.

[53] A. Mohamed, A.K. Anas, A.B. Suriani, A.A. Azira, M. Sagisaka, P. Brown, J. Eastoe, A. Kamari, N.H. Hashim, I.M. Isa, Preparation of multiwall carbon nanotubes (MWCNTs) stabilised by highly branched hydrocarbon surfactants and dispersed in natural rubber latex nanocomposites, Colloid Polym. Sci. 292 (11) (2014) 3013–3023.

[54] A. Mohamed, A.K. Anas, A.B. Suriani, T. Ardyani, W.M.W. Zin, S. Ibrahim, M. Sagisaka, P. Brown, J. Eastoe, Enhanced dispersion of multiwall carbon nanotubes in natural rubber latex nanocomposites by surfactants bearing phenyl groups, J. Colloid Interface Sci. 455 (2015) 179–187.

[55] K. Singh, A. Ohlan, P. Saini, S.K. Dhawan, Poly (3, 4-ethylenedioxythiophene)/Fe_2O_3 polymer composite-super paramagnetic behavior and variable range hopping 1D conduction mechanism synthesis and characterization, Polym. Adv. Technol. 19 (3) (2008) 229–236.

[56] N. Rattanasom, S. Prasertsri, K. Suchiva, Mechanical properties, thermal stability, gas permeability, and phase morphology in natural rubber/bromobutyl rubber blends, J. Appl. Polym. Sci. 113 (6) (2009) 3985–3992.

[57] J. Brandrup, E.H. Immergut, W. McDowell, Polymer Handbook, Wiley, 1975.
[58] N. Norhakim, S.H. Ahmad, C.H. Chia, N.M. Huang, Mechanical and thermal properties of graphene oxide filled epoxy nanocomposites, Sains Malays. 43 (4) (2014) 603–609.
[59] A. AnsÃ³n-Casaos, J.A. PuÃ©rtolas, F.J. Pascual, J. Hernandez-Rerrer, P. Castell, A.M. Benito, W.K. Maser, M.T. Martanez, The effect of gamma-irradiation on few-layered graphene materials, Appl. Surf. Sci. 301 (2014) 264–272.
[60] R. Stephen, S. Jose, K. Joseph, S. Thomas, Z. Oommen, Thermal stability and ageing properties of sulphur and gamma radiation vulcanized natural rubber (NR) and carboxylated styrene butadiene rubber (XSBR) lattices and their blends, Polym. Degrad. Stab. 91 (8) (2006) 1717–1725.
[61] B. Dehghanzad, M.K.R. Aghjeh, O. Rafeie, A. Tavakoli, A.J. Oskooie, Synthesis and characterization of graphene and functionalized graphene via chemical and thermal treatment methods, RSC Adv. 6 (5) (2016) 3578–3585.